Chapter 4: **Volcanic eruptions on Mars and lava flow morphology and thermodynamics**

Authors: Caitlin Ahrens, Vincenzo Cataldo, and Giovanni Leone

4.1 Introduction

It is almost impossible to think of a volcano without contemplating the power displayed during an eruption. Mars has a variety of volcanism as displayed in this book, and therefore reflect the varied processes that shaped them, and with a wide range of plumbing systems, supply rates, magma types, and eruption styles. Understanding eruptive styles and hypotheses on such mechanisms represents a distinct geophysical process on the Martian surface and subsurface. On the surface as imaged by numerous spacecraft, such as Mariner 9, Viking, and most recently the Mars Reconnaissance Orbiter (MRO), are diversities in the ancient lava flows, leading to discussions on the pyroclastic activity [1-9].

Whenever magma is produced by partial melting at depth, it will have a tendency to ascend to the surface as long as its density contrast with the surrounding materials is to essentially produce a positive buoyancy [10, 11]. Like Earth's volcanism, the ascent may occur in stages, with the magma pausing to form intrusive bodies (i.e., dikes, sills) which may undergo chemical and physical evolution. These evolutions may then lead to a diversification of eruptions and product compositions [1, 10]. One approach to understanding the styles of Martian volcanic activity has been to compare the morphologies with those of terrestrial analogs [10, 12, 13]. While useful for basic generalization, this method may overlook potentially dramatic effects between terrestrial and Martian environments on eruptive processes [14-16]. Wilson and Head [10] suggest that considering the initial processes of ascent and eruption of magma on Mars would lead to predictive analyses on the types of volcanic landforms. On the evaluation of the crustal configuration of Mars and a theoretical perspective of the ascent and eruption of magma through this crust in the Martian gravitational and atmospheric conditions, the Martian environmental conditions operate to modulate the various eruptive styles (this chapter) and morphology of the resulting landforms (see Chapters 1 and 9).

The objective of this chapter is to outline our current understanding of the eruption styles on Mars. This includes the different types of eruptions (from gas-free flows to eruptive pyroclastic activity) that may have been present on Mars, intrusive mechanisms, and the periodic activity related to magma reservoirs and the presence of calderas. We also explore the thermodynamics of lava flow morphology.

4.2 Eruption Styles

The range of eruption styles similar to terrestrial volcanoes have a common denominator – gas exsolution from magmas at shallow depth, which depends on factors such as composition, volatile content, and temperature (which controls magma rheology), and

environmental settings (i.e., atmospheric pressure and gravity) [14, 17, 18]. The terminology for Martian eruption types is essentially and conveniently identical to eruptions on Earth [1, 10, 19]. However, we emphasize that the classifications are based on physical processes, not necessarily on the eruption deposits or landforms produced [14, 17, 20]. Wilson and Head [10] state that there are two events that may occur as a volatile-bearing magma nears the surface and the total pressure decreases. The first critical event is gas nucleation, where gas bubbles begin to nucleate if the amount of the volatile present is enough to ensure some small degree of supersaturation before the magma reaches the surface. Martian lavas have a typical volatile content of ~0.5 wt% water, ~0.7 wt% carbon dioxide, and ~0.14 wt% sulfur dioxide, and several other constituents [10, 21, 22]. The second critical event is magma disruption, where the magma may disrupt into a mixture of released gas and pyroclastics if the volatile content is relatively greater [see 14, 23]. In essence, whenever a steadily erupting magma contains adequate volatiles to ensure that it disrupts into pyroclasts, the kinetic energy produced by expansion of the released gas warrants pyroclasts and gas emergence from the vent at eruption speeds of at least a few tens of meters per second [10, 15, 24].
In steady explosive eruptions, the style is determined by a combination of the size distribution of pyroclasts and the mass fraction of released volatiles in the eruption products. These factors control the degree of coupling between the motions of clasts and gas. Large clasts have a larger terminal fall velocity through the gas than smaller, same-density clasts, and higher-density clasts have a larger terminal velocity than lower-density clasts. As a result, [25] states that there is a maximum size of clast of a given density which can be transported out of the vent.

4.2.1 Gas-free

There is little disruption of the magma and its exit velocity is small (< 10 m s^{-1}; < 1 m s^{-1} for mafic magmas) comparable to the velocity it would have had due to buoyancy or excess pressure forces [21, 26] if it had been volatile-free. In such cases, magma overflows quietly from the vent, forming a low, domelike fountain, most possibly only a few meters high, and feeds directly into a lava flow (Figure 1).

4.2.2 Strombolian

This is considered a special case when a gas/volatile-poor magma rises at a low speed and the coalescence of gas bubbles to occur in the rising magma, which can vary from passive degassing to violent fire fountaining [27, 28]. When large bubbles rise buoyantly faster than smaller bubbles, a runaway process can occur in which large bubbles emerge intermittently from the vent [10, 29], through a “puffing” action [29, 30] to more eruptive processes [31, 32]. This sweeping of a vertical column of magma nearly clean of other bubbles describes the strombolian eruption style (Figure 1). The magma then erupts quietly during the intervals (one to tens to seconds) between the explosive emergence of the large gas bubbles [27, 26, 33].

4.2.3 Hawaiian

Hawaiian eruptions tend to occur in mafic magmas when most of the magma is disrupted into clots not much smaller than the maximum eruptible size, which decouples quickly from the gas to form a fountain of material and fall relatively near the vent (Figure 1). Through this fountain process, the accumulating clasts depend on their sizes and passage out of the fountain [20, 26]. Three possible clast formations may occur: (i) cold enough to form brittle scoria deposits; (ii) hot enough to form spatter deposits; (iii) uncooled to coalesce into a lava pond which can feed one (or more) lava flows.

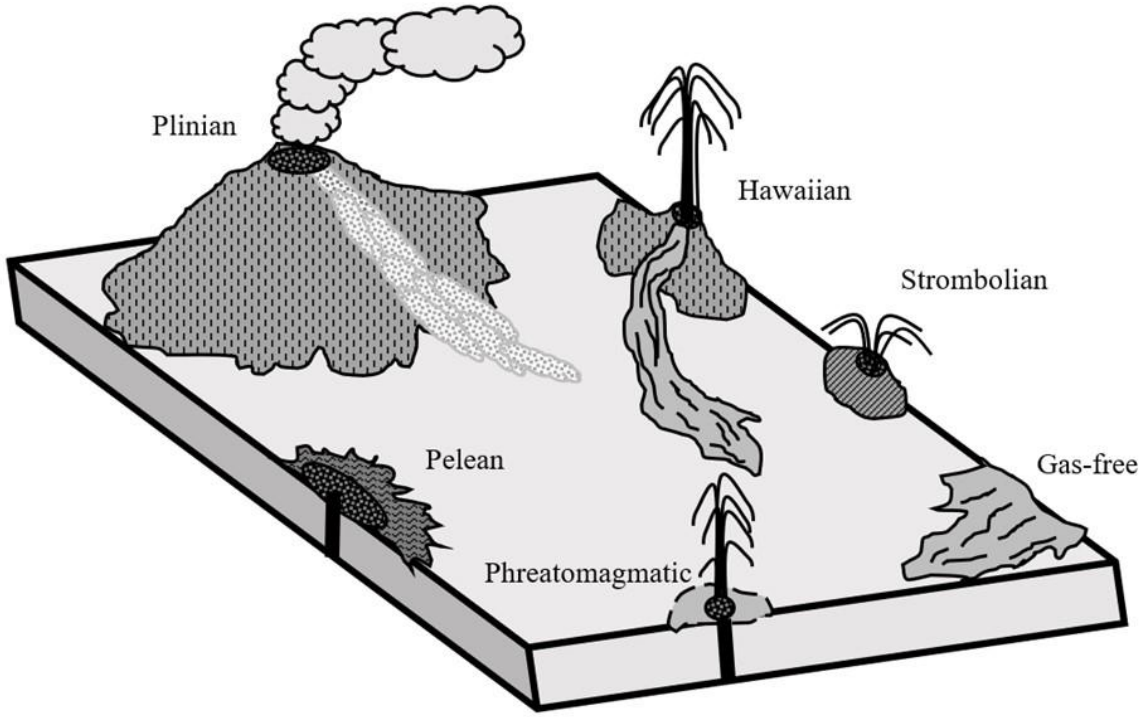

Figure 1: The swath of physical processes occurring in the vicinity of a vent on Mars can result in a wide array of eruption styles, as shown. (*Counterclockwise*): Gas-free magma erupts to produce low, fluid feeding flows; Strombolian eruptions are due to gases exceeding magma ascension speeds, causing bubbles to grow and coalesce and lava to spatter; Hawaiian eruptions are steady explosive eruptions, creating a pyroclastic fire fountain; Plinian eruptions are due to fragmented magma locked into a gas stream, contacting a convecting atmosphere and spread laterally, or pyroclastic flows (ignimbrites) stream down slopes; Pelean eruptions occur when low magma rise speed causes cooling and forms a viscous dome with pyroclastic flows; Phreatomagmatic eruptions are the solidification of magma and gas buildup in a localized conduit, causing an explosive disruption. Adapted from [10].

4.2.4 Plinian

Unlike Hawaiian eruptions, Plinian eruptions can occur in any magma type (Figure 1). However, the stipulation is that most of the magma that disrupts into clots must be small

enough that they are effectively locked by drag forces to the venting gas [10]. Fundamentally all of the eruption products ascend into an eruption cloud over the vent, provided the bulk density of such eruptions products become less than the density of the atmosphere (as a result of the heating of atmospheric gases) [10, 14, 21]. Interesting to note from [25] is that small pyroclasts can transfer heat efficiently to the atmospheric gases entrained into the eruption cloud and thus maximize buoyant convection of the eruptive cloud into the atmosphere.

Differences in the atmospheric pressure and temperature structure cause Plinian eruption clouds to rise ~ 5x higher than terrestrial clouds for the same eruption rate [10], although it is speculated that eruption clouds pose similar cloud-height and deposit-width relationships on Mars as on Earth. A consequence of the lower Martian atmospheric pressure is that Martian Plinian deposits of any magma composition will be systematically finer-grained than those on Earth (by a factor of ~ 100 in sub-cm size) [10, 17]. Large-scale Plinian deposits, though mainly of basaltic composition [17], may be linked to the enhanced fragmentation of basaltic magma (rather than silicic) in the Martian environment, or to the interaction of basaltic magma with groundwater. However, silicic-type Plinian eruption styles must have a sufficiently large magma volatile content enough for thorough distribution of the magma around the vent. Thus if the magma had both low viscosity and sufficiently low rise velocity through the lithosphere, then gas bubble coalescence could be significant enough to lead to a more intermittent explosive style, consisting of a more coarse pyroclastic grain distribution [34].

4.2.5 Pelean

The main characteristic of pelean explosions (Figure 1). is that the maximum excess pressure in the trapped gas is limited (≤ 10 MPa) by the tensile strength of the retaining cooled exterior [10, 24]. For magmas of intermediate–basaltic to silicic composition, it is common that the rise speed of the magma nearing the surface is relatively small. This leads to extensive cooling of the magma in contact with the fissure walls in the form of an extrusive dome. These factors, along with the efficient retention of gases released from the decompressing magma, can lead to the slow accumulation in the interior of a near–surface magma body (or extrusive dome) of a substantial pressure (more so than the local hydrostatic pressure) [10]. The eventual failure in tension of the cooled retention exterior leads to the explosive decompression of the gas, which drives the pelean eruption style [35].

4.2.6 Phreatomagmatic

The interaction between magma and ground ice has been supported to explain various (and notably unusual) landforms of possible volcanic origin on Mars, including: massive pyroclastic deposits; large-scale ground collapse and chaotic terrain; major outflow channels; lahars; sub-ice-sheet eruptions; pseudocraters; landslides on volcanic edifice flanks; and hydrothermal sites [22, 36, 37, 38, 39].

Phreatomagmatic explosions appear to be the consequence of the interaction of juvenile material with near-surface layers of ice volatiles [10, 17, 40, 41]. These types of eruptions (Figure 1) differ from pelean mainly in that coarse, non-juvenile, lithic material is incorporated into the ejecta. Phreatomagmatic volcanism is highly expected on Mars, particularly at the Hrad Vallis, Granicus Valles, and Hebrus Valles regions, due to the presence of significant amounts of near-surface ices in many regions [10, 42, 43, 44, 45, 46, 47, 48] whereas pelean activity would occur if/when high-viscosity magmas approach the surface.

4.3 Effusive activity

The term *effusive* in volcanology refers to the non-explosive extrusion of magma at the surface, which includes all eruptions of lava flows, coulees, and domes. As previously discussed, a number of factors must be taken into account for the wide variety of effusive activity, such as environmental temperatures, pressures, and gravity; composition; volatility; porosity and other rheological characteristics. Several studies in recent years have involved the relationship between lava flow morphology to both rock chemistry and eruption mechanism through rheological physics [7, 49, 50, 51; see Section 4.7 of this Chapter]. Martian samples through landers have found that samples from Chryse Planitia [6, 52] and Utopia Planitia [6, 52] show ~44 wt.% SiO_2, ~19 wt.% Fe_2O_3, and lesser amounts of Al_2O_3, MgO, and SO_3. It should be noted that the amount of SiO_2 is critical in the general thickness, discharge rate, and ultimately flow of the lava, where relatively higher levels (> 55 wt% SiO_2) would typically be andesitic or dacite composition, much larger thickness and slower discharge rate [53]. These types are comparable to the terrestrial analogues at Trident, Alaska and Hibok-Hibok, Philippines [53]. Lower levels of SiO_2 are basaltic/basaltic andesitic, with smaller thicknesses and faster discharge rate, and comparable to terrestrial sites like Etna and Vesuvius, Italy [53]. From a photo geological standpoint, a number of lava flow morphologies have been identified [Figure 2; 6, 10, 51]. This section will review the variety of volcanic features with associated lava flow morphology and lava flow morphology across volcanic plains.

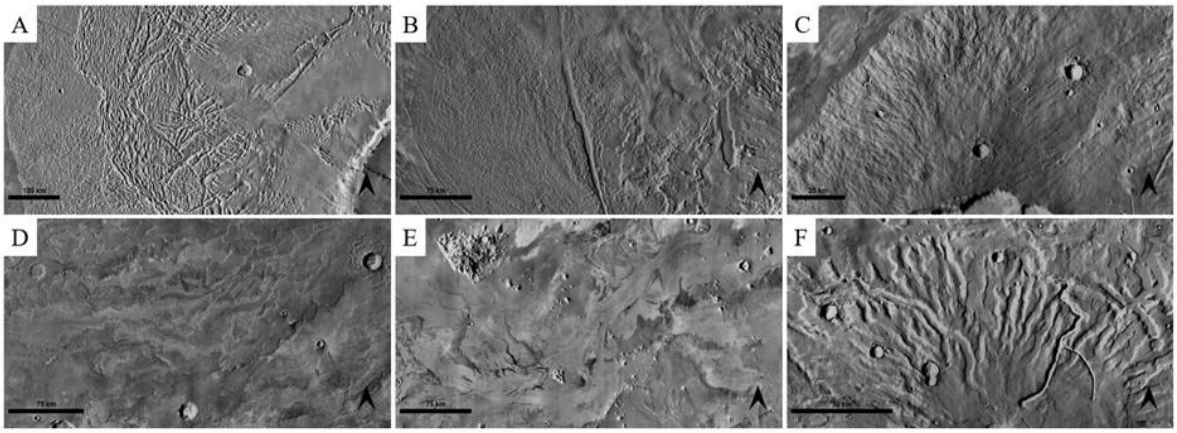

Figure 2: Sampling of lava flow morphologies across various volcanic constructs on Mars as imaged by the THEMIS camera. A) Olympus Mons (scale bar = 100 km); B) Arsia Mons (scale bar = 75 km); C) Uranius Tholus (scale bar = 25 km); D) Daedalia Planum (scale bar = 75 km); E) Elysium Mons (scale bar = 75 km); F) Tyrrhena Patera (scale bar 50 km).

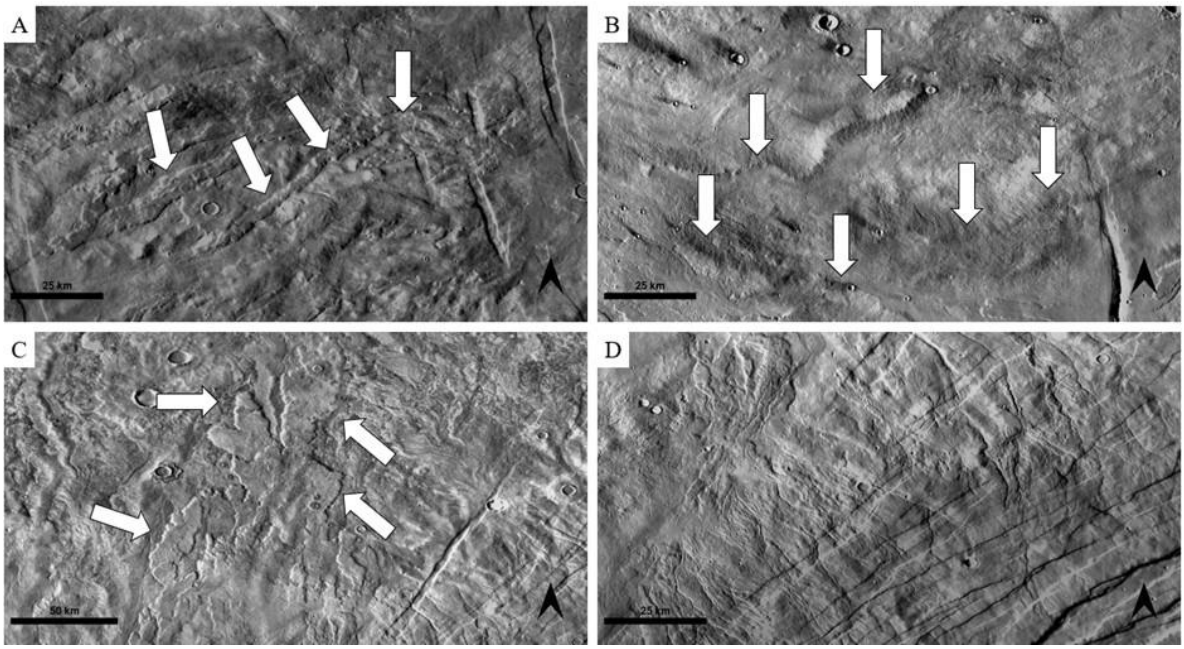

Figure 3: THEMIS observations of various Alba Patera flows at its western and northwestern flanks. A) Tube-channel flows (scale bar = 25 km); B) Tube-channel flows (scale bar = 25 km); C) Sheet flows (scale bar = 50 km); D) Undifferentiated flows (scale bar = 25 km).

4.3.1 Central volcanoes

Past images from the Mariner 9 orbiter showed a variety of volcanic and volcanic-related features described primarily on the basis of their topographic profiles and include: (i) tholii (domes with steep slopes); (ii) shields; (iii) patera; and (iv) a host of small (~1 km) positive relief features considered to be cinder cones. Shields were compared to shield

volcanoes on Earth, and thus interpreted to be composed essentially of basaltic lavas; tholii were then representative of more viscous, possibly silicic lavas.

Alba Patera does not fit into this category and tends to be its own classification [54, 55]. However, Alba Patera displays a diversity of lava flows that make up the structure. Four main lava flows are identified [3, 54, 55]: tube-fed and tube-channel flows; sheet flows; and undifferentiated flows (Figure 3).

Tube-fed and tube-channel flows are characterized by radial-centric ridges to the center of Alba Patera (Figures 3a and 3b). Lava channels and partially-collapsed tubes can be outlined down the axes of the flows that were considered to be the main conduits feeding the advancing flow [54]. Lava tube construction in comparison with terrestrial and lunar environments have basaltic rheological properties. More silicic lavas are too viscous, or extremely fluid lavas also do not seem to develop tubes [6, 56, 57, 58]. The width of the tubular flows around Alba Patera are only representative of the exposed part of the flow. From terrestrial counterparts, lava channels and tubes form constructional arches along their axes, principally by overflow and ultimately act as topographic barriers [54, 59], with the potential of subsequent flows burying the lower flanks of the arch or not able to breach the arch. Because of this, it is possible to determine the actual width of the tube-fed flows. However, the incidence angle plus the exposed portion of the flows as a minimum can estimate a flow volume [54]. Comparing such volumes to typical effusion rates of basaltic lavas on Earth gives some consideration on the curiousness on Alba. It should be noted that many flows appear to have operated essentially concurrently, either with extremely high rates of effusion or the eruptions were of very long duration. [54] favors the latter interpretation due to the lack of lava tube formation from high effusion rates (flood eruptions) on Earth, therefore Alba tube-fed flows may have developed through the eruption of basaltic lavas of moderate rates of effusion over many years of activity [55, 60, 61]. Other features that may be present in tube-fed flows are domes at the terminus of the flow, which may be the result of lava flowing within the tube system from the vent under hydrostatic loading. At the lower end of the flow, the lava may rupture the tube roof (forming a pseudo-vent) and resulting in local sprouting of flows to build up into domes [62].

Sheet flows are the most noticeable type of lava flows on Alba Patera (Figure 3c). The actual vents for the sheet flows are not visible, where they may have been buried by their own effusive products, though appear to originate near the ring fracture. Typically sheet flows lack flow surface structures, such as tubes and channels, but form multiple, overlapping lobes of material. The relationship between the rate of effusion and length of the lava flows suggests that the sheet flows involve high rates of effusion, possibly comparable to terrestrial flood eruptions [54].

The fourth type of flow observed at Alba Patera are the undifferentiated flows (Figure 3d). Although many of these flows are initiated by tubes and channels, they differ by having surfaces of rugged relief and indistinct flow margins [54]. It is also apparent that from the superposition relations and their levels of degradation that the undifferentiated flows at the distal ends of Alba Patera may be the oldest flows [54, 55]. Yet, the undifferentiated flows within the ring fractures are fresh appearing with well-defined channels with levees, though some cut by caldera-originated fractures, which implies a contemporaneous eruption-caldera formation sequence. The combinations of these flow types all over the vicinity of Alba Patera suggest that this volcanic region involved both

flood-type eruptions (from a central region) and Hawaiian styles over long durations [54, 61].

4.3.2. Highland Patera

This sub-category of central volcano includes Tyrrhena Patera, Hadriaca Patera, and the Amphitrites Patera complex [5; see Chapter 10]. These features are all distinguished by their low profile, radial channels, and complex central calderas. It has been proposed by several studies [63] that some of the channels on Tyrrhena Patera are primarily formed by ash eruptions along with some levels of erosion by wind, subsurface volatiles, and mass wasting [Figure 2f; see Chapter 10]. Flood lavas of the nearby and greater Hesperia Planum encroached and partly buried the flanks of Tyrrhena Patera, as observed by flow contacts through erosional channels and other depressions. From previous studies [6, 64], the last stage of volcanism at Tyrrhena Patera is the eruption of a small volume of lava in the central volcanic region, producing upper shield materials and lava channels to supply plains materials from the Tyrrhena summit [6, 54].

4.3.3 Shield volcanoes

The shield volcanoes of the Tharsis region provided the first clear evidence from orbital data that volcanism was quintessential in the evolution of Mars. This category of volcano is characterized by central vent(s) often in the form of complex calderas, and composed of numerous overlapping flows (and flow units), many of which are fed by lava tubes and channels. The main Martian shield volcanoes occur in the Tharsis region (Figures 2a, 2b, 2c, 2d), Elysium region (Figure 2e), and southeast of Elysium (Apollinaris Patera region) [see Chapters 1, 9, and 10]. Many of the flows appear to originate from the shields, where some cases the flanks are buried by lava flows from younger volcanoes (or unidentified sources) [54]. Although the details of the flows (and sequences thereof) vary from shield to shield, all have a complex history and share the same general morphology. The steep slopes of shield volcanoes could result from several factors, including: (i) increased proportion of pyroclastics in relation to lavas; (ii) decreased rate of effusion, producing relatively shorter lava flows; and (iii) more silicic compositions that produce more viscous flows [54, 57].

4.3.4 Dome volcanoes

Domes, or tholii, on Mars are characterized by relatively steeper slopes than the aforementioned shield volcanoes, usually exceeding ~8° in slope. The notable steepness of the domes is attributed to more viscous lavas, higher proportion of pyroclastics, lower rates of effusion, or a combination of these factors. The surface texture of these dome structures range from relatively featureless and smooth (Tharsis Tholus) to higher relief lava flows and channels (Ceraunius Tholus). However, these features are usually buried (or partly buried) by younger lava flows erupted from adjacent lava plains vents or

mantled material of non-volcanic origin, which suggests an older geological age of these domes [54].
Along with the more viscous lavas, this leads to a more felsic-based composition. This was a geomorphologic case for felsic volcanic domes in western Arcadia Planitia (eastern Phlegra Montes) [65, 66], and felsic spectral signatures across volcanic features at the Nili Fossae caldera and Terra Sirenum [67, 68, 69]. These felsic domes are morphologically similar to terrestrial felsic volcanic domes by the presence of concentric structures, lava injections, viscous flows, and summit fissures [66]. These domes have the potential to form in the subsurface as *cryptodomes*. While domes are associated with lobate aprons and aureoles, [65] suggests that "pancake"-shaped domes (similar to the terrestrial "torta" domes found in the Andes [70]) were extrusive or partially extrusive, and that extrusive boulders were formed by autobrecciation – the process whereby volatile-bearing extruded magmas fragment when exposed to the lower pressure surface.

4.3.5 Volcanic Plains

These plains make up for roughly 60% of the surface area of Mars. Many of these smooth regions are of volcanic origin, though several criteria are used to classify these as actual volcanic lava flows. These include surface morphology, such as: lava flow fronts; embayment relations suggesting fluid emplacement; and mare-type wrinkle ridges [1, 2]. The volcanic plains are categorized into four broad groups based on more detailed and distinct morphological differences.
The first classification is the simple flow plains. Simple flow plains display low relief, and numerous mare-type wrinkle ridges, typically found in Hesperia Planum. This unit also appears to consist of a thick sequence of lavas [6, 54]. Simple flows may have been emplaced as flood lavas, extruded at extremely high rates though long fissure vent systems that spread rapidly, thus resurfacing extensive regions [54, 55, 61]. Therefore, this process is primarily important as basin-filling and highland-resurfacing. Type examples are the Hellas, Argyre, and Isidis basins that are filled with simple flows.
The second type of volcanic plain are complex flows. These are particularly found in the vicinity of the Tharsis bulge, displaying a complex of overlapping flow lobes and lack wrinkle ridges. This type also includes some of the youngest lavas on Mars, though there are indicators of flow-lobed lava plains to be found among the oldest plains on Mars [71]. This suggests that the presence of flow lobes is an indicator of emplacement rather than a result of erosion [54]. To distinguish from the simple flows, complex flow plains result from a style of volcanism involving more protracted, sporadic, and lower rates of effusion. Although relatively higher flows in comparison to Hawaiian-type, shield-building rates, the complex flows are composed of compound, overlapping flow units of comparable thickness [72].
The third type of volcanic plain are the undifferentiated flow plains. These are classified by a lack of widespread features with the exception of a few, scattered features such as flow lobes. [54] state this classification is loosely defined and may include aeolian or periglacial relations, particularly in the northern latitudes [3, 73]. This type of volcanic plain is rather heavily based on their proximity to well-defined volcanic regions, such as the Tharsis region [74, 75].

Werner [54] includes a possible fourth classification of volcanic plains labelled the "*questionable*" plains. These plains are extensively modified by fracturing, mass wasting, and erosional processes. Some of these peripheral to the Tharsis bulge are heavily fractured and almost certainly older that have been modified by such faulting. Other regions of interest with this type of volcanic plain are at the aureoles of the Tharsis volcanoes, where origins are uncertain, but could include volcano-clastic debris, such as mud and ash flows [76, 77]. There are also numerous areas of questionable plains surrounding the Elysium complex, modified by complex tectonic and channeling processes [6, 78, 79].
In summary, volcanic plains being the majority of the Martian surface leads to implications of the phreatic activity on Mars, given the presence of volatiles within the regolith [21, 80, 81].

4.3.6 Leveed lava flows

Leveed lava flows have an interesting emplacement history, as observed by several previous studies [82, 83, 84]. Such flows on Mars (also on the Moon and Earth), deposit a significant amount of active lava volume into stationary components (e.g., levees or margins). Terrestrial analogues [85, 86, 87, 88] and experimental experiments [89] indicate that levees are established as the front flow passes, and that additional products to the levees continue long after the frontal lobe has passed. The flow front leaves a stationary deposit along the margins of the flow to establish essentially a channel, yet subsequent clogs and breakouts occur upstream, adding additional material to the levee [82]. On Mars specifically, it is difficult to tell from morphology alone to distinguish these processes dominating levee formation. However, this flow emplacement process can lead to differences in volumetric flow rate, duration of emplacement, and certainly the rheology of the lava over time. Such examples of leveed lava flows can be observed at the Tharsis volcanoes, Arsia (Figure 2b), Pavonis, and Ascraeus Mons [82].

4.4 Intrusive activity

As we have explored eruption styles and lava flow types across the Martian surface, the conditions for flow and eruption physics also extend to the subsurface where the movement of magma ascension through the Martian rock layers can also depend on gravity/isostasy, composition, density, viscosity, and rheology. Because of the Martian lower gravity environment, fluid convective motions and settling processes driven by buoyancy forces, as well as overall diapiric ascent rates, will be slower on Mars than on Earth [10, 90]. This ascension process, along with the lower gravity on Mars, causes cooling-limited flows to be longer (nearly 6x longer on Mars), and also favors an increase in dike widths on Mars (by a factor of 2) and subsequently higher effusion rates (by a factor of 5) [10]. With the lower Martian gravity and lower atmospheric pressure, this ensures that both nucleation and disruption of magma occur at greater depths on Mars than on Earth, although lava flow cooling rates and surface textures would be relatively the same. Heat is conducted out of the magma into the dike walls during dike emplacement. In the subsurface aquifer system, heated volatiles are incorporated into

the magma as vapor bubbles [91, 92]. Conservatively, the estimate of the rate at which heat penetrates laterally is found by assuming that no convection occurs, therefore heat transfer is then limited by the thermal diffusivity of the dike wall material [91].

The propagation of magma-filled dikes and cracks from magma source regions often concludes in the dike reaching the surface to cause eruption of the magma and production of lava flows. Commonly, dikes (or portions thereof) approach the surface but do not reach it, setting up an extensional near-surface stress field that does produce consequential surficial fractures and graben [93]. Long graben systems are then evidence for lateral dike swarms radiating from major volcanic centers, where the upper part of the dikes is trapped at shallow depths by the regional stress field and magma density [93]. Wilson and Parfitt [94] and Wilson and Head [95] addressed the influence of gravity on dike widths and eruption rates. It was found that dike propagation is limited by the dike tip stresses must overcome the effective fracture toughness of the country rocks. This implies that the mean width of a dike should be inversely proportional to the cube root of the acceleration due to gravity, and its length perpendicular to the direction of magma motion should be inversely relational to the gravity raised to the 2/3 power [10]. Flow velocities of laminar-motion-oriented magmas in dikes are proportional to the total pressure gradient and square of the dike width; whereas in more turbulent motion, the velocity is proportional to the square root of the product between the pressure gradient and dike width [10]. From this, the upper limit on magma ascent speed is set by the mean width of the widest dike that can be formed in a given stress field [10].

Density, as well as other factors, can exert controls on the upward migration of plumes and magma material. Ascending diapirs may stall upon encountering rheological barriers of cooler – more viscous – surroundings, such as the outer thermal boundary layer [10]. If the magma is still buoyant, instabilities may develop in the source region, or the viscous lid and small diapirs may ascend. Depending on the rheological properties of the country rock, diapirs may propagate from the stalled diapir or deep magma reservoir [10, 96].

There are several clues of intrusive activity across the surface of Mars. [46] observed intrusive-generated surface flows in the region around Hrad Vallis, and dike formations around Olympus Mons [97] and Cerberus Fossae [93]. In the NW area of Elysium Planitia, [46] observed some clues to dike-fed sill intrusions around ridged mountains, similar to hyaloclastic ridges in Iceland. It was postulated that these ridges formed as a consequence of a dike rising close to the surface and intruding a sill, though no explosive decompression of the sill took place, quite possibly due to a lower substrate volatile content. With the observance of additional narrow ridges running along the long axis of the mountains suggests that a dike approached close to the surface before the mountain-building production [46].

The emplacement of lateral dikes extending to significant distances (> 2000 km) from Olympus Mons may be linked to the latest caldera collapsing processes, and that the last phase of summit inflation was insufficient to initiate further dike intrusions [97, 98]. From this possible connection, there may be a minimum-volume-limited threshold for dike emplacement and caldera collapse. At the smaller Tharsis region volcanoes, the volumes of the lateral dikes are greater than that of large paterae, probably due to the magma being “buffered” within the edifice [98, 101, 102] or that any magma chamber was only partially emptied [97]. These dike intrusions could occur at the end-life of a

magma chamber when the creation of a large dike rising from the mantle inflates the magma chamber to the point where multiple ruptures can happen [97]. Therefore, not only is a lateral dike initiated, the stresses on the overlying rocks cause caldera collapsing to begin.

The presence of subsurface ice (along with more felsic, silicic materials) could also influence intrusive volcanic interactions and form cryptodomes and "brain terrain" [66, 103], most notably in western Arcadia Planitia [104, 105]. Volcano-ice interactions have also been described on the northern plains of Mars [38, 39] and in the Sysiphi Montes region in the southern hemisphere [106, 107]. As noted by Farrand et al [108], the past presence of ice in the Arcadia Planitia region is indicated by the brain terrain surface texture, a texture similar to those found in mid-latitude lobate debris aprons (LDAs) [109, 110, 111, 112]. More discussion on this issue will be provided in Chapter 9.

4.5 Magma reservoirs

The lithospheric structure of Mars has been well studied by a variety of techniques [10, 16, 39, 61, 113]. [113] inferred a mean global thickness of (basaltic) crust of 34 – 40 km, with maximum thicknesses under Tharsis (61 – 77 km) and minimum thicknesses under Hellas (8 – 10 km). This thickness from the upper mantle strongly suggests upper mantle source regions may have an evolutionary trend of compositions as a function of time and degree of upper mantle depletion [10]. Systematic thickening of the Martian lithosphere as a function of time from thermal history models [114] estimates that lithospheric thicknesses from the tectonic response to individual loads show spatial and temporal variations in elastic thickness, with distinctly lower values beneath major volcanic provinces [115].

As stated earlier, the lower gravity on Mars plus positive/negative buoyancy forces will consequently have slower diapiric ascension rates. The differences in both gravity and surface atmospheric pressure, in addition to the differences in lithospheric bulk density, result in magma reservoirs to be deeper on Mars than on Earth by a factor of ~4 [10, 116]. Thus although lithospheric thickness generally increases as a function of time, thus influencing the position of the brittle-ductile transition and level of diapiric rise versus dike emplacement, prolonged regional volcanic phases can ultimately affect the regional thermal gradient [117]. Wilson and Head [10] also assume that the basic processes controlling partial melting of mantle materials (and magma segregation] at depth on Mars is similar to processes on Earth, occurring as a result of adiabatic decompression of the ascending mass, and gradients in density, compaction, or deviatoric stresses [118, 119]. Such thermal inhomogeneities cause localized regions of the mantle to ascend diapirically, and the sizes, shapes, and spacings of these regions (and their ascent rates) are determined by the overall advective heat flux, along with the physical properties of the volcanic bodies and environmental material [120, 121, 122]. Wilson et al [123] argue that any one magma reservoir can survive as a thermal entity so long as it is supplied with source-region magma at a sufficient rate that its contents remain largely molten (not a high accumulation of crystallization). Once the fluid cools to ~25% crystals, it will cease to act as a Newtonian fluid and behave rheologically as a more solidified one [124].

Shallow magma chambers are extended by the injection of melt from below. The melt bodies rise buoyantly from deeper zones of partial melting as diapirs or elongated dikes. Each newly implemented melt body added to the existing reservoir brings a finite volume and internal pressure in excess of the ambient lithospheric pressure. Therefore, the reservoir reflects a constant flux (readjusting) between its internal volume and stress state of the surrounding rocks [125]. For substantial cooling to occur in an existing reservoir (of any given size), there must be a significant reduction of magma supply from the mantle or relatively long period of time. This in itself implies periodicity in the magma supply rate from the mantle [123]. As the reservoir contents cool and solidify, denser crystals sink to the bottom, and the overall density of the contents increases due to thermal contraction. The reservoir will then adjust to a new gravitational equilibrium by sinking to a deeper level within the density-stratified edifice to be neutrally buoyant [126], increasing the vertical and radial stress component beneath the lower portion of the magma reservoir and decreasing the stress around the upper part of the reservoir [127].

Relatively deep magma reservoirs can form in several different mantle environmental settings, which we will review here. Some result from the fusing of a rising diapir (or hotspot) as the adiabatic temperature reaches the melting point curve, as well as voluminous pressure release melting occurs, producing a large, partially molten magma source region [10]. Deep reservoirs are also concurrent with rift zones on Earth as a result of crustal thinning, localized mantle upwelling, and pressure release melting. Rift zones that on Mars do not exist due to the lack of plate tectonics. Commonly, magma reaches shallow levels where it achieves a neutral buoyancy with the country rock due to the decreased density of the shallow crustal materials [10].

If sufficient material reaches this level, a secondary reservoir is possible, as is observed at the Kilauea volcano on Earth [128]. These secondary magma reservoirs evolve with their centres at neutral buoyancy levels [123, 128, 129], where at depths of the magma density is equal to the density of the country rocks. Generally, silicate compositions (and thus phases) expand on melting, and so positive buoyancy of the magma in the lower portion of a chamber is expected [57]. Negative buoyancy may be due to several factors, including shallow layers in the country rock to likely consist of ancient lava flows, ash deposits, and other low-density material [10].

4.6 Caldera types and associated processes

Calderas are large, sometimes irregular depressions, the diameter of which is many times greater than that of included subsurface vents. The basic formation of calderas are by way of a roof collapse over an underlying shallow magma reservoir, though their shape and morphology vary depending on several factors, including composition, flow rate of the subsiding magma, depth of the magma chamber, roof geometries, and environmental setting. Generally, the caldera diameter increases in proportion to volume of the associated eruption.

Buoyant rise of the magma body may cause broad uplifting and therefore production of ring and radial fractures. Volcanic leaks from the evolving magma chamber commonly produce multiple clusters of vents over the magma chamber, at times in linear or arcuate

patterns [130]. However, some of this pre-collapse morphology may sometimes be covered during the caldera-collapse event.

There are a variety of tell-tale signs of a caldera collapse. These geomorphological features serve as a general basis of a caldera, though more complex subsidence and multi-collapse events may highly morph the overall structure. The topographic rim is simply the top of the escarpment that bounds the caldera, enclosing both the subsidence area and the area of scarp retreat due to rock falls and mass wasting [130]. Next is the inner topographic wall, which is typically the steepest in its upper portions and tends to have a concave profile that flattens downslope. Material removed by mass wasting and scarp retreat defines a collapse collar. Arcuate bounding faults (arcuate ring faults) are exposed at some deeply eroded volcanic areas (> 5 km in diameter). These can also accommodate uplift as well as subsidence [130]. Most observed ring faults are near-vertical or dip steeply inward. Such the geometry and placement of the ring faults may also reflect sequential change, from an early stress field related to magma withdrawal to later stresses related to slumping. Some sizeable calderas can lack bounded arcuate ring faults, but limited erosion depths preclude unambiguous interpretation. The next geomorphic structure typical of calderas is the intra-caldera fill. This provides key evidence of caldera processes because collapse occurs during associated eruption events, and ignimbrites and inter-leaved caldera breccias accumulate to multi-kilometre thicknesses within the subsided area. The distribution of such accumulations can influence the timing and geometry of subsidence [130]. The caldera floor geometry and overall shape can give a lot of evidence on the eruptive and post-eruptive processes. We will review the different types of caldera subsidences and their diversity of geometry.

4.6.1 Subsidence Processes

The complexity of Martian calderas gives rise to the variety of types of processes for such collapse events to take place. Size of the eruption and geometry of the subsurface magma chamber are also valuable factors for differing subsidence developments. We briefly review the types of subsidence that may occur for different caldera-forming processes [see also 130].

Many large calderas dominantly involve *plate* (or *piston*) collapse, which consists of a coherent floor bounded by steeply dipping faults. These are mainly from a single, large volume eruption. *Trapdoor* subsidence, bounded by an incomplete arcuate fault and by a hinged segment, reflecting early or incomplete downsagging and plate collapse. In the subsurface, this type may also include an asymmetric intrusive system or magma chamber. Simple *downsag* subsidence is fairly rare, containing inward-tilted blocks along their margins. These also require a smaller volume, though much deeper intrusive dike or magma chamber system. Terrestrial volcanoes, such as Kilauea and Mauna Loa, are notable downsag calderas that have become multi-cyclic. A component of the *piecemeal-fault* disruption of caldera floors is common, although such structures so not usually accommodate the bulk of subsidence in larger calderas. However, the caldera floors are not usually simple and smooth, more likely relating to a multicyclic nature [130]. Brecciated *chaotic* disruption of subsiding caldera floor and the *funnel* type can be identified to smaller (< 3 – 5 km in diameter) calderas. Chaotic subsidence has been proposed to generate low-density material within calderas that can account for the

observed negative gravity, and to generate lithic breccias by collapse of the rood over a depressurizing magma chamber. Funnel-types are associated with explosive eruptions from a central vent, lacking a bounding ring fault (or subsiding blocks), and of more mafic magma to form tuff rings and maars.

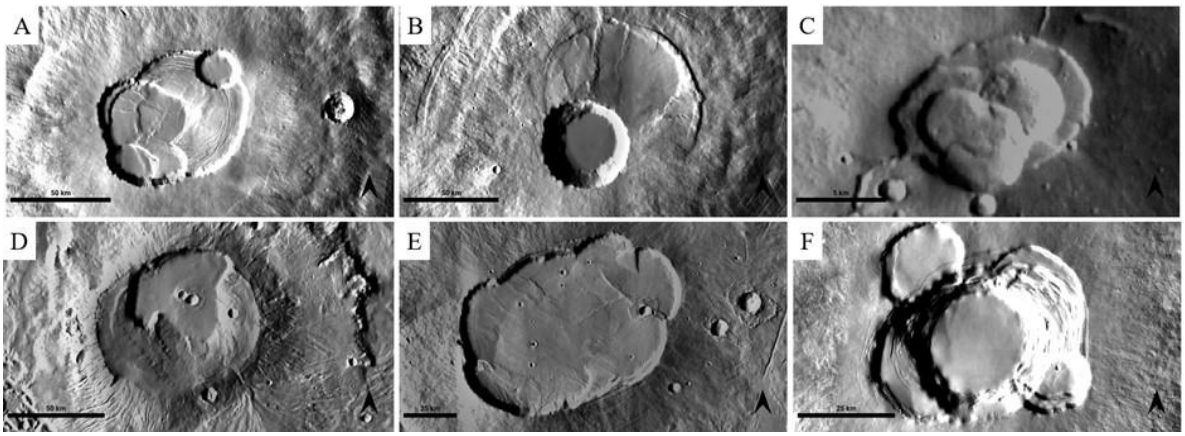

Figure 4: Caldera complexities across the surface of Mars as imaged by THEMIS. A) Olympus Mons nested caldera complex (scale bar 50 km); B) Pavonis Mons simple caldera (scale bar 50 km); C) Hecates Tholus nested complex (scale bar 5 km); D) Apollinaris Patera downsag or multicyclic caldera (scale bar 50 km); E) Uranius Tholus smooth-floored, scalloped-rim caldera (scale bar 25 km); F) Ascraeus Mons with multi-arcuate ring fractures (scale bar 25 km).

4.6.2 Martian Caldera Types

4.6.2.1 Shields

The prominent shield volcanoes of the Tharsis region have at least one summit caldera. Several nested calderas are visible on the summits of Olympus Mons (Figure 4a), Ascraeus Mons (Figure 4f), and Alba Patera [16, 123,131], and all show evidence for at least one caldera collapse event. This variety of summit caldera morphologies have been classified by several previous studies [123, 132, 133, 134].

Both Ascraeus and Olympus Mons have multi-sets of summit calderas, consisting of a central caldera with smaller ones located around its margin. Arsia and Pavonis Mons (Figure 4b), the two major southerly Tharsis volcanoes do not show this complexity in multi-caldera summit morphology. Instead, Arsia Mons has a single large caldera, and Pavonis Mons has a sag-like depression with small collapse pitting. These calderas infer the presence of shallow magma reservoirs, fed by batches of small rising magma from the mantle, within which magma resided for some time before expulsion to form either an intrusion, an extrusive lava flow, or pyroclastic flow [128]. The existence of a single caldera collapse, let alone multiple collapse depressions, implies that at least once (and then possibly several times) during the lifetime of each reservoir, a sufficiently large

volume of magma was withdrawn in that the stresses of the roof exceeded the country rock strength, allowing subsidence to take place [123; 135].

Olympus Mons is by far the most morphologically complex caldera as observed on Mars. It has been noted that as much as a 2.5 km of collapse took place within the 80 x 65 km diameter caldera [136], with an elevation difference of about 2.0 km (low elevations around the oldest collapse depressions). Tectonic features on the caldera floor indicate an extensional (graben) environment around the perimeter to transition to a more compressional (ridge) formation. This transition occurs at a radial distance of ~17 km from the caldera center, which is important to note considering that this may infer the magma chamber to be relatively shallow, nearly ≤ 16 km beneath the caldera floor [137]. There is also evidence found within the Olympus Mons caldera for solidified lava lakes more than 30 km in width and for the localization of withdrawal of lava within the lakes [136]. Mouginis-Mark [138] identified both compressional and extensional features on the floor of the Olympus Mons complex (see Chapter 9). These include compressional ridges (1 – 3 km wide) that are morphologically similar to lunar wrinkle ridges, and narrower (< 1 km wide) linear ridges approximately circumferential to the perimeter of the caldera crater.

Mouginis-Mark and Robinson [136] have remarked that there is an eight-stage evolutionary sequence for the Olympus Mons caldera subsidence and found that it was a long-term process rather than near-instantaneous events from comparable terrestrial examples. The proposed sequence of deformation has been well-estimated by multiple image data collected by a number of Mars missions, including the Viking 1 Orbiter, Mars Express, Mars Global Surveyor, and Mars Reconnaissance Orbiter.

The following observations of the Olympus Mons complex have been inferred in the following stages:

(1) The first preserved summit event was the catastrophic collapse and subsequent partial infilling, which essentially defines the caldera boundary. Post-collapse talus is interpreted to be presently buried beneath younger materials.

(2) Continuation of subsidence of the central portion of the caldera crater, which created an extensional environment close to the caldera wall and a compressional environment closer to the caldera centre. Concentric graben and ridges formed at this stage as well.

(3) New collapse events occurred at the western part of the caldera, forming a 1700-m deep crater. After the solidification of the floor of this newly formed crater, an episode of circumferential graben formed close to the caldera wall, presumably due to the subsidence of the floor centre.

(4) To the south of the caldera centre, additional new subsidence events formed. These events postdate the formation of the main caldera due to the cross-cutting relationships of the graben and scarp boundaries.
(5) Resurfacing (burial of earlier tectonic features and the creation of a smooth caldera floor) by a large lava lake during (or just after) its formation. The linear ridges are interpreted to be compressional, produced by local convergence (or rafting) of solidified lava plates on the surface of the lava lake.
(6) This stage consists of the partial drainage of the lava lake, producing a topographic relief "bench."
(7) Continued subsidence of the central portion of the summit area produce a compressional stress regime [137] that promoted the formation of the larger (> 3 km wide) wrinkle ridges. The numerous wrinkle ridges formed from the partial drainage in Stage 6 were thus preserved on top of these larger wrinkle ridges.
(8) The final collapse event. Unlike the preservation of events from Stage 5, there is no evidence of surface features (i.e., linear ridges and wrinkle ridges of large-scale subsidence or deformation) that could be associated with upending of the lake on the floor.

However, there are alternative hypotheses to explain the observed ~2 km variation in rim topography of the Olympus Mons nested caldera complex and the younger segments were built to higher elevations. Mouginis-Mark and Robinson [136] suggest that the original caldera formed off-centre, similarly to what has occurred at Mauna Loa, Hawaii. Another option is that the intrusive events associated with continued activity raised the rim crest where activity continued the longest, although extensional graben would be expected, but no such features are observed. Alternatively, one side of the summit area may have subsided relative to the other, while younger lava flows bury bounding faults, like that at Kilauea volcano, Hawaii [13, 139]. The commonality with all these hypothetical caldera-forming sequences and partial caldera infilling demonstrates that Olympus Mons underwent similar summit activity to Hawaiian volcanoes [127].
These collapse events at Olympus Mons may have spanned thousands to a few millions of years [99, 140], but there is still insufficient data to constrain the exact timing and duration of this complex activity. All of the volcanic events are implied to occur in a relatively short time period compared to the entire geologic history of Mars (over 4 billion years) [140].

4.6.2.2 Paterae and Tholi

Alba Patera has been considered a patera type volcanic construct [3], but also considered a shield [5] or a unique volcanic type all on its own category [6]. Although its edifice shape is certainly peculiar (although much wider and lower than any Martian shield), the caldera is essentially shield-like, similar to Uranius Tholus (Figure 4e). There is little topographic relief, and the highest point is not the centre but part of the fractured perimeter [141, 142], reminiscent of Mauna Loa, Hawaii.
Highland paterae have very low relief with complex calderas, with incised radial channels at their flanks [5, 6; see Chapter 10]. The lack of radial channels at volcanoes with obvious lava flows at shields and domes suggests that the paterae are composed of

pyroclastic materials. The Apollinaris Patera edifice stands about 5 – 6 km in relief and 200 km in diameter at its base [143]. The summit of Apollinaris has at least two separate calderas (Figure 4d). The outer-seeming caldera is larger than the nested calderas of the Tharsis calderas at Olympus (Figure 4a), Ascraeus (Figure 4f), and Pavonis (Figure 4b). Episodic eruptions and caldera formation could have taken place throughout the growth of the edifice [144]. The size of a caldera, as discussed earlier, increases with the volume of eruption materials, though the link between eruption volumes and caldera diameters are not that straight-forward due to infilling and erosion [144, 145, 146]. Apollinaris is thought to have been active during the early to mid-Hesperian [147], composed mainly of low-viscosity lavas or pyroclastic deposits [148, 149, 150].

Hecates Tholus (Figure 4c) is another example of complex caldera formation of paterae and tholi structures [34; 151] and is the northernmost of the three volcanic constructs in the Elysium Planitia region. Lack of impact craters indicates a very young age for this eruption, possibly even postdating the most recent collapse episode at the Olympus Mons caldera complex ~ 300 My [34, 152]. The summit of Hecates Tholus is characterized by a nested caldera nearly 11.3 x 9.1 km in extent. At least four distinct caldera collapse events are evident, with the maximum caldera depth to be ~470 m. Unlike the larger Tharsis shields that show evidence of lobate lava flows on their flanks [3, 7], Hecates has no flow features of this type. However, the sinuous rilles are similar to those at Uranius and Ceraunius tholi [63], possibly by-products of erosion from volcanic density currents [63; 153]. Craters observed on the flanks of Hecates give an approximate age of 1680 ± 326 – 3600 ± 38 My [5, 34]. Mouginis-Mark et al [34] analysed Hecates Tholus and suggested that the Hecates deposit was produced by a relatively steady, Plinian explosive eruption. As mentioned earlier in this chapter, the Plinian eruption style is associated with silicic magmas with a sufficiently large magma volatile content enough for thorough distribution of the magma in and below the vent.

4.7 Thermal properties and erosional power of lava

Several studies have involved efforts to relate lava flow morphology to rock chemistry and eruption mechanisms through consideration of the rheological properties of the lava itself [6, 7, 154, 155, 156]. This section defines the rationale for a three-dimensional model of thermal erosion mechanisms and rheological mechanisms by lava flows.

4.7.1 Rationale for Creation of a Three-Dimensional Model of Thermal Erosion by Lava

[157] created the first 3-D model of thermal erosion by turbulently flowing lava on the Moon to assess how channel bank erosion relates to erosion at the channel bed, something that has never been addressed before by existing one- and two-dimensional models. When applied to sinuous rilles or curved channels in general, a 3-D model has the unique advantage of revealing the details of flow circulation and how flow velocity, viscosity and pressure at meander bends relate to the same flow parameters at the channel centerline and bed. *How does flow circulation at meander bends vary when varying temperature distribution within the lava? Will the details of flow circulations be*

the same for crusted versus uncrusted flows? The lava that flowed within a sinuous lava channel might have either been crusted over (though a similar assumption is hard to reconcile with a fully turbulent flow regime) or might have lost heat by radiation (on a planetary body like our Moon, which lacks an atmosphere) or radiation/convection (on a planet like Mars). Alternatively, it might have flowed insulated and this likely caused it to reach greater downstream distances from the lava source. These different emplacement environments compel us to describe a range of possible scenarios and explore how different vertical distributions of lava temperature for each scenario might have related to the details of flow circulation at the channel bed and banks. The other advantage of a three-dimensional model lies in its ability to reveal spatial variations of erosion rates with changing flow rate, flow temperature, and meander/channel geometry.

4.7.2 Open source Field Operation And Manipulation (OpenFOAM)

The [157] model uses the resources made available by OpenFOAM, a C++ library of applications called solvers and utilities. Solvers enable simulation of specific problems of Computational Fluid Dynamics (CFD), whereas utilities are designed to perform simple pre-and post-processing tasks like those involved in mesh generation. The OpenFOAM finite volume software is extremely versatile because users can create their own solvers and utilities or modify existing ones. Among the solvers that are used in turbulence modeling and are available in OpenFOAM, “simpleFoam” was chosen for the purpose of simulating steady-state flow scenarios. The software allows for grid design that can be tailored to the scenario of interest. Several meshes of curved channels of different length and width and with meanders of different wavelength and amplitude were generated to simulate flow.

4.7.3 The Finite-Volume Method

A thorough description of the method is found in [158]. The term finite volume refers to the small volume surrounding each node point in a mesh. Analogous to other numerical methods developed for the simulation of fluid flow, the finite volume method transforms a chosen set of partial differential equations into a system of linear algebraic equations. The discretization process involves two basic steps: in the first step, the partial differential equations are integrated and transformed into conservation equations over an individual volume or cell. In the second step, interpolation profiles are chosen to approximate the variation of the variables within the cell and relate the surface values of the variables to their cell values. This later step leads to the algebraic equations previously mentioned.
A key advantage of this methodology is the fact that the flux entering a given volume is identical to that leaving the same volume, i.e. the method is conservative. Furthermore, a key ingredient in the implementation of the methodology is setting up the geometrical support framework for the problem at hand, which also allows for unstructured meshes.

4.7.4 Turbulence Modeling

The motion of a turbulent lava flow – an incompressible fluid – can be described by the Navier-Stokes momentum equations in the x, y, and z direction. To reduce the large computational cost associated with a direct solution of the Navier-Stokes equations, statistical analyses can be used to simplify the resolution of turbulent flows. Specifically, the time-dependent nature of turbulence together with its wide range of time scales suggest that statistical averaging techniques can be applied to approximate fluctuations. The process of time-averaging introduces two new unknowns (Reynolds stresses) into the system of equations, and is applicable to Netwonian fluids only because Reynolds stresses are assumed to be a linear function of the mean velocity gradients [158]. The process of calculating Reynolds stresses is referred to as turbulence modeling and consists of finding two additional transport equations. Two among the most widely used turbulence models are the k-epsilon and SST k-omega models. Each of the two models contains two additional transport equations. The standard "k-ε" model [159, 160] is a high Reynolds number model that does not perform well in cases of adverse pressure gradients and flow separation. The k expression quantifies the turbulent kinetic energy that is produced, convected, and diffused within the flow, and the ε equation approximates turbulent dissipation. The "SST k-ω" model [161] switches to a "k-ε" behavior in the free stream, and can be used as a low Reynolds number model all the way down to the wall, thanks to the Shear Stress Transport (SST) formulation. Omega is the rate of dissipation of the turbulent eddies or, in other words, the rate at which turbulence kinetic energy is converted into internal thermal energy per unit volume and time [158]. Thanks to SST formulation, the SST k- ω model is very well-suited to determine erosion rates into the lava substrate and is especially effective in cases of adverse pressure gradients and flow separation.

4.7.4.1 Modifying SimpleFoam – The OpenFOAM Steady-State Solver for Turbulent Flow

Although the [157] model adopts an initial value of flow velocity at the lava source (inlet value in the three directions, U_x, U_y, and U_z), the velocity field within the flowing lava is not known and has to be computed by solving the set of Navier-Stokes equations. For incompressible flows, this task is complicated by the strong coupling that exists between pressure and velocity and by the fact that pressure does not appear as a primary variable in either the momentum or continuity equations [158]. The Semi Implicit Method for Pressure Linked Equations (SIMPLE) algorithm was specifically designed to reformulate the Navier-Stokes equations in terms of a momentum and a pressure equation, which are then discretized and solved sequentially. The sequence is repeated until the velocity and pressure fields satisfy both mass and momentum conservation [162]. The simpleFoam solver that is made available in the OpenFOAM library is well-suited for the purpose of modeling turbulent, incompressible flow. The key input parameters of the flow are velocity and pressure, and flow is investigated in steady conditions. However, no initial temperature is specified in the solver, a severe limitation when modeling turbulently flowing lava.

To solve the temperature limitation inherent in the solver, [157] coupled a 3-D temperature model to simpleFoam. The first step was to choose an energy expression that could be applicable to a fixed control volume and fit a scenario of turbulently flowing lava. An energy equation can be written in terms of specific internal energy, specific enthalpy, specific total enthalpy, or temperature. An energy expression written in terms of temperature assumes that the flow is Newtonian because the specific enthalpy of the flow is only a function of pressure and temperature variations [158]. Such an assumption is consistent with a scenario of turbulently flowing lava for which lava temperatures are assumed to be above at or near the liquidus value. Finally, our steady-state energy expression as a function of temperature can be written as:

$$\nabla \left[\rho\, c_p\, v\, T\right] = \nabla\, [k\, \nabla T] \qquad \text{Eq. (1)}$$

in which ρ is density of the liquid lava, c_p is lava specific heat capacity, **v** is the velocity vector (**v** = v_x, v_y, v_z), T is lava temperature, and k is lava thermal conductivity. Because we are dealing with an incompressible fluid, lava density is taken as a constant. If we normalize Eq. (1) by density, we obtain:

$$\nabla \left[\, c_p\, v\, T\right] = \nabla \left[\frac{k}{\rho}\, \nabla T\, \right] \qquad \text{Eq. (2)}$$

Conveniently, the lava *effective thermal diffusivity* α_{eff} can be expressed as a function of lava thermal conductivity, k, as follows:

$$\alpha_{eff} = \frac{k}{\rho\, c_p} \qquad Eq.(3)$$

If we solve for k and then substitute (3) into (2), we obtain:

$$\nabla \left[\, c_p\, v\, T\right] = \nabla \left[\, c_p \alpha_{eff} \nabla T\, \right] \qquad \text{Eq. (4a)}$$

or

$$\nabla\, [v\, T] = \nabla \left[\, \alpha_{eff} \nabla T\, \right] \qquad \text{Eq. (4b)}$$

The left-hand side term in (4a) is a convection term and the right-hand side one is a diffusion term and they are both normalized by density. Eq. (4b) represents the temperature model that was coupled to the SimpleFoam solver, and the suffix “eff” stands for effective. The *effective thermal diffusivity* accounts for the laminar and turbulent components of diffusivity, and is given by:

$$\alpha_{eff} = \frac{\upsilon}{PrPr + \alpha_t}$$ Eq. (5)

in which υ is the kinematic viscosity of the lava, Pr is the molecular (laminar) Prandtl number and α_t is the kinematic turbulent thermal diffusivity that is expressed as:

$$\alpha_t = \frac{\upsilon_t}{Pr_t}$$ Eq. (6)

4.7.5 Deriving an expression for erosion rate of the lava substrate

The one-dimensional expression that allows determination of the erosion rate into the lava substrate, u_m, is obtained by adopting the approach taken by [163, 164, 165, 166], as follows:

$$u_m = \frac{h_T(T_l - T_m)}{\rho_g[c_g(T_m - T_0) + L_g]}$$ Eq. (7)

in which the numerator represents the convective heat flux to the base of the flow and the denominator defines the energy required to melt the ground. Specifically, h_T is the convective heat transfer coefficient, T_l is the temperature of the liquid lava, T_m is the temperature of melting of the ground, ρ_g is the density of the lava substrate, c_g is the substrate specific heat capacity, T_0 is substrate temperature away from the lava/substrate interface, and L_g is latent heat of fusion of the ground. Equation 7 calculates the steady-state rate of advance of the ground/lava interface, when thermal equilibrium is assumed at the lava/ground interface.

To find an expression that can be used in our model, we must equate the numerator of Eq. (7) to a heat flux expression that contains thermal diffusivity and temperature gradient of the lava in a direction perpendicular to the lava/substrate interface, as follows:

$$h_T(T_l - T_m) = -\rho c_p \alpha_{eff} \frac{\partial T}{\partial n}$$ Eq. (8)

in which the left-hand side term represents the convective heat flux to the base of the flow and $\frac{\partial T}{\partial n}$ is the temperature gradient of the lava in a direction perpendicular to the channel bed and banks. The convective heat transfer coefficient [166] can be expressed as:

$$h_T = \frac{0.027\ k\ Re^{0.8} Pr^{0.33}}{h}\left(\frac{\mu_b}{\mu_g}\right)0.14$$ Eq. (9)

in which Re is the Reynolds number of the flow, expressed as:

$$Re = \frac{U\,L}{\upsilon} \quad \text{Eq. (10)}$$

in which U is flow velocity, L is the characteristic length of the flow (here the hydraulic diameter of the channel) and υ is the kinematic viscosity of the lava. In Eq. (9), h is lava thickness, μ_b is the bulk dynamic viscosity of the flow and μ_g is the dynamic viscosity of the lava substrate. Equation 9 shows how the value of the heat transfer coefficient is influenced by flow thickness, and also accounts for the viscosity of the substrate. By combining (8) and (7), we obtain:

$$u_m = \frac{-\rho\, c_p\, \alpha_{eff}\, \frac{\partial T}{\partial n}}{\rho_g[c_g(T_m - T_0) + L_g]} \quad \text{Eq. (11)}$$

which is used to calculate erosion rates into the channel bed and banks. In the following section, we will describe the key input parameters and assumptions of the [157] model. This will help identify the flow parameters in (9) that are most effective in determining variations in erosion rate.

4.7.6 Model input parameters and assumptions

The input parameters of the [157] model can be divided into physical, thermo-physical and turbulence parameters of the flowing lava. Among the physical parameters, the model requires initial flow velocities or velocities at the channel inlet. The temperature of the lava at time of eruption is also another key input parameter. The model adopts the [168] temperature-dependent viscosity that – though it was originally used for the purpose of investigating flow behavior in the Bingham laminar regime – can be used to model the evolution of lava temperature and viscosity as long as flow rate is fixed (a scenario for which flow height and velocity are both independent of lava yield stress and flow regime is Newtonian [168]. The vertical distribution of temperatures within the flow is similar to that modeled by previous authors [169, 170], with higher temperature values at the flow top and core and lower values at the channel bed. Lava temperature and viscosity at the channel banks are assumed to be the same as those at the channel bed. The actual temperature values at the channel bed and banks were chosen based on how convective heat flux is transported to the base of the flow. Holding the initial lava temperature and viscosity equal, the higher the flow thickness the higher the convective heat flux to flow boundaries, i.e., the value of the left-hand side term of Eq. (8). As a result, the temperature gap occurring between the flow top (and core) and the boundaries will be greater for a thicker flow. As lava temperature decreases, viscosity increases at both the channel bed and banks.

The [157] model assumes steady-state flow conditions, an assumption justified by the likely long-lasting duration of eruptive events associated with the formation of sinuous rilles [171]. The lava substrate is modeled as consolidated and unconsolidated, depending on available information at individual flow sites.

4.7.7 Erosional evolution

Erosional processes may have a potential to lead to interesting characterizations of the evolution of volcanic-related features, such as pitting, fossae, and chasmata [see Chapter 5 for further discussions on volcanic channels and fracturing]. Deep chasmata and steep-sided depressions typical at Tharsis and Elysium, particularly in Labyrinthus Noctis [172] and Valles Marineris [173, 174], in combination with volcano-tectonic processes, showcase possible hypotheses of lava tubes, pit chains, and fossae evolutions [175]. [175] noted that although tectonism and faulting related to magma movements and presence of dike swarms, as noted earlier in this chapter, could be plausible in volcanic activity, erosional processes related to lava tube collapse and consequent movement of fluids explain the evolution of such pit chains into chasmata.

Initially, lava erupting to the surface and injected underground erodes its own pathways to form lava tubes (such as the area between Pavonis Mons and Labyrinthus Noctis), where the erosion is thermally-dependent and can extend down into pre-existing surface materials. Notably at Labyrinthus Noctis, curvilinear pit chains are not observed to be associated with visible faults [175], though they are formed by the collapse of lava tubes [176, 177]. Exactly uphill along the direction of the main Labyrinthus Noctis – Valles Marineris axis, tube-fed flow fields between Arsia and Pavonis Montes are observed [175]. Initial chasmata at the western portion of Valles Marineris are connected to the eastern end of Labyrinthus Noctis [175]. Kasei Valles nearby also shows bifurcated pit chains that suggest subsurface lava circulation. Parallel to Kasei Valles, Maja and Shalbatana Valles show outflow channels that decrease their size with increased distance away from Tharsis [175]. All of these locations are just a small portion of Martian volcanic areas that show a variety of lava-induced erosional features. Whether the lava flooding has cyclic and subsequent episodes or a steady flow, this process can further erode pit chains and widen them into fossae, and continuously erode to larger structures like valles and chasmata (see Chapter 5).

4.8 Summary

In this chapter we summarized the present state of knowledge on Martian magma reservoirs, consequent eruption styles, lava flows and caldera processes, and the rheological implications of lava flow dynamics using current modeling techniques. These processes are essential to understanding the geologic foundations of Martian volcanism and evolution of varying volcanic constructs across the Martian surface. Despite the many years of analysis, many outstanding questions regarding the construction of these various volcanoes (including paterae and tholii) remain, such as

those concerning the transition from explosive to effusive activity. Importantly, the [157] model presented in this chapter has the potential to reveal how fluid- and thermodynamic parameters relate to variations in erosion rates throughout an entire curved/sinuous channel, something that was never addressed in previous work. In conclusion, we hope that this chapter will be used as a guide to explore in more detail the mechanics of eruption, magma rising, volcanic construction, and lava flow generation and evolution.

References

[1] Carr, M. (1973), Volcanism on Mars; Journal of Geophysical Research, 78 (20), 4049 – 4062.

[2] Carr, M., and Clow, G., (1981), Martian channels and valleys: Their characteristics, distribution, and age; Icarus, 48 (1), 91 – 117.

[3] Carr, M., Greeley, R., Blasius, K., Guest, J., Murray, J., (1977), Some Martian volcanic features as viewed from the Viking orbiters. JGR, 82 (28), 3985 – 4015.

[4] Greeley, R. (1973), Mariner 9 photographs of small volcanic structures on Mars. Geology, 1 (4), 175-180.

[5] Plescia, J., and Saunders, R., (1979), The chronology of the martian volcanoes; 10th Lunar and Planetary Science Conference Proceedings, vol. 3, 2841-2859.

[6] Greeley, R., and Spudis, P. (1981) Volcanism on Mars; Reviews of Geophysics and Space Physics, 19 (1), 13 – 41.

[7] Schaber, G., Horstman, K., Dial, A., (1978), Lava flow materials in the Tharsis region of Mars; 9th Lunar and Planetary Science Conference Proceedings, vol. 3, 3433-3458.

[8] Schaber, G. (1982), Syrtis Major: A low-relief volcanic shield; Journal of Geophysical Research: Solid Earth, 87 (B12), 9852-9866.

[9] Hodges, C., and Moore, H., (1994), Atlas of volcanic landforms on Mars; US Government Printing Office, (No. 1534).

[10] Wilson, L., and Head, J., (1994), Mars: Review and analysis of volcanic eruption theory and relationships to observed landforms; Reviews of Geophysics, 32 (3), 221-263.

[11] Black, B., and Manga, M., (2016), The eruptibility of magmas at Tharsis and Syrtis Major on Mars. JGR Planets, 121 (6), 944-964.

[12] Gulick, V., and Baker, V. (1990), Origin and evolution of valleys on Martian volcanoes; JGR Solid Earth, 95 (B9), 14325-14344.

[13] Seelos, K., Arvidson, R., Jolliff, B., Chemtob, S., Morris, R., Ming, D., Swayze, G. (2010), Silica in a Mars analog environment: Ka'u Desert, Kilauea Volcano, Hawaii. Journal of Geophysical Research: Planets, 115 (E4).

[14] Wilson, L., and Head, J. (1983), A comparison of volcanic eruption processes on Earth, Moon, Mars, Io and Venus; Nature 302, 663 – 669.

[15] Wilson, L., (1984), The influences of planetary environments on the eruption styles of volcanoes, Vistas Astron., 27, 333-360.

[16] Mouginis-Mark, P., Wilson, L., Zuber, M. (1992), The physical volcanology of Mars; In: Mars, edited by H. H. Kieffer, B. M. Jakosky, C. W. Snyder, and M. S. Matthews, University of Arizona Press, Tucson, 424-452.

[17] Wall, K., Rowe, M., Ellis, B., Schmidt, M., Eccles, J. (2014), Determining volcanic eruption styles on Earth and Mars from crystallinity measurements. Nature Communications, 5, 5090, 1-8.

[18] Houghton, B. F. et al. (2004), The influence of conduit processes on changes in style of basaltic Plinian eruptions: Tarawera 1886 and Etna 122 BC. J. Volcanol. Geotherm. Res. 137, 1–14.

[19] Fisher, R., and Schmincke, H. (1984), Pyroclastic Rocks, 472 pp., Springer-Verlag, New York.

[20] Head, J., and Wilson, L. (1986), Volcanic processes and landforms on Venus: Theory predictions and observations; J. Geophys. Res., 91, 9407-9446.

[21] Craddock, R., and Greeley, R. (2009), Minimum estimates of the amount and timing of gases released into the martian atmosphere from volcanic eruptions; Icarus, 204 (2), 512-526.

[22] Kusanagi, T., and Matsui, T. (2000), The change of eruption styles of Martian volcanoes and estimates of the water content of the Martian mantle; Physics of the Earth and Planetary Interiors, 117 (1-4), 437-447.

[23] Sparks, R. (1978), The dynamics of bubble formation and growth magmas: A review and analysis; J. Volcanol. Geotherm. Res., 3, 1-37.

[24] Wilson, L., (1980), Relationships between pressure, volatile content and ejecta velocity in three types of volcanic explosion, J. Volcanol. Geotherm. Res., 8, 297-313.

[25] Wilson, L., (1976), Explosive volcanic eruptions, III, Plinian eruption columns, Geophys. J. R. Astron. Soc., 45, 543-556.

[26] Wilson, L., and Head, J. (1981), Ascent and eruption of basaltic magma on the Earth and Moon; J. Geophys. Res., 86, 2971-3001.

[27] James, M., Lane, S., Wilson, L., Corder, S., (2009), Degassing at low magma-viscosity volcanoes: Quantifying the transition between passive bubble-burst and Strombolian eruption; J. Volcanology and Geothermal Research, 180 (2-4), 81-88.

[28] Parfitt, E., and Wilson, L. (1995), Explosive volcanic eruptions – IX. The transition between Hawaiian-style lava fountaining and Strombolian explosive activity. Geophysical Journal International, 121 (1), 226-232.

[29] Harris, A., and Ripepe, M. (2007), Temperature and dynamics of degassing at Stromboli; Journal of Geophysical Research-Solid Earth, 112 (B3).

[30] Ripepe, M., Harris, A., Carniel, R. (2002), Thermal, seismic and infrasonic evidences of variable degassing rates at Stromboli volcano; Journal of Volcanology and Geothermal Research, 118 (3-4), 285-297

[31] Chouet, B., Hamisevicz, N., McGetchin, T. (1974), Photoballistics of volcanic jet activity at Stromboli, Italy; Journal of Geophysical Research, 79 (32), 4961-4976

[32] Blackburn, E., Wilson, L., Sparks, R. (1976), Mechanisms and dynamics of strombolian activity; J. Geol. Soc. London, 132,429-440.

[33] Parfitt, E. (2004), A discussion of the mechanisms of explosive basaltic eruptions; Journal of Volcanology and Geothermal Research, 134 (1-2), 77-107.

[34] Mouginis-Mark, P., Wilson, L., Head, J. (1982), Explosive volcanism at Hecates Tholus, Mars: Investigation of eruption conditions; J. Geophys. Res., 87, 9890-9904.

[35] Eichelberger, J., and Hayes, D. (1982), Magmatic model for the Mount St. Helens blast of May 18, 1980, J. Geophys. Res., 87, 7727-7738.

[36] Head, J. W., and Wilson, L. (2002). Mars: a review and synthesis of general environments and geological settings of magma-H2O interactions. Geological Society, London, Special Publications, 202(1), 27-57.

[37] Schulze-Makuch, D., Dohm, J., Fan, C., Fairén, A., Rodriguez, J., et al. (2007). Exploration of hydrothermal targets on Mars. Icarus, 189(2), 308-324.

[38] Allen 1979 Allen, C. C. (1979). Volcano-ice interactions on Mars. Journal of Geophysical Research: Solid Earth, 84(B14), 8048-8059.

[39] Chapman, M., Allen, C., Gudmundsson, M., Gulick, V., Jakobsson, S., et al. (2000), Volcanism and ice interactions on Earth and Mars; Environmental effects on volcanic eruptions, Springer, Boston, MA, pp. 39-73.

[40] Self, S., Wilson, L., Nairn, I. (1979), Vulcanian eruption mechanisms, Nature, 277, 440-443.

[41] Brož, P., and Hauber, E. (2013), Hydrovolcanic tuff rings and cones as indicators for phreatomagmatic explosive eruptions on Mars; Journal of Geophysical Research: Planets, 118(8), 1656-1675.

[42] Clifford, S. M. (1981), A pore volume estimate of the Martian megaregolith based on a lunar analog. In: 3rd International Colloquium on Mars (Vol. 441, p. 46).

[43] Clifford, S. M. (1984), A model for the climatic behavior of water on Mars; UMass Dissertations, Scholarworks.

[44] Clifford, S. M. (1993), A model for the hydrologic and climatic behavior of water on Mars. Journal of Geophysical Research: Planets, 98(E6), 10973-11016.

[45] Squyres, S. W., Clifford, S. M., Kuzmin, R. O., Zimbelman, J. R., Costard, F. (1992), 16: Ice in the Martian Megaregolith. In: Mars. pp. 523-554.

[46] Wilson, L., and Mouginis-Mark, P. J. (2003), Phreatomagmatic explosive origin of Hrad Vallis, Mars; Journal of Geophysical Research: Planets, 108(E8).

[47] De Hon, R. A. (1992), Martian lake basins and lacustrine plains; Earth, Moon, and Planets, 56(2), 95-122.

[48] Mouginis-Mark, P. J. (1985), Volcano/ground ice interactions in Elysium Planitia, Mars; Icarus, 64(2), 265-284.

[49] Baloga, S. M., Mouginis-Mark, P. J., Glaze, L. S. (2003), Rheology of a long lava flow at Pavonis Mons, Mars; Journal of Geophysical Research: Planets, 108(E7).

[50] Bleacher, J. E., Greeley, R., Williams, D. A., Cave, S. R., Neukum, G. (2007), Trends in effusive style at the Tharsis Montes, Mars, and implications for the development of the Tharsis province; Journal of Geophysical Research: Planets, 112(E9).

[51] Crown, D., and Ramsey, M., (2017), Morphologic and thermophysical characteristics of lava flows southwest of Arsia Mons, Mars; Journal of Volcanology and Geothermal Research, 342, 13-28.

[52] Toulmin, P., Baird, A., Clark, B., Keil, K., Rose, H., et al. (1977), Geochemical and mineralogical interpretation of the Viking inorganic chemical results; J. Geophys Res., 82, 4625-4634.

[53] Killburn, C. (2000) Lava flows and flow fields; In: Encyclopedia of Volcanoes, Sigurdsson, H., et al. (eds.), Academic Press, p. 291 - 307.

[54] Werner, S. C. (2009). The global martian volcanic evolutionary history. Icarus, 201(1), 44-68.

[55] Cattermole, P. (1990), Volcanic flow development at Alba Patera, Mars. Icarus, 83 (2), 453-493.

[56] Greeley, R., (1977), Basaltic 'plains' volcanism, Volcanism of the Eastern Snake River Plain, Idaho, NASA Contract. Rep., CR-154621, 23-43.

[57] Skok, J., Mustard, J., Ehlmann, B., Milliken, R., Murchie, S., (2010), Silica deposits in the Nili Patera caldera on the Syrtis Major volcanic complex on Mars; Nature Geoscience, 3, 838-841.

[58] Francis, P., and Wood, C. (1982), Absence of silicic volcanism on Mars: Implications for crustal composition and volatile abundance; J. Geophys. Res. 87, 9881-9889.

[59] Greeley, R. (1971), Observations of actively forming lava tubes and associated structures, Hawaii, Mod. Geol., 2, 207-223.

[60] Mouginis-Mark, P. J., Wilson, L., Zimbelman, J. R. (1988), Polygenic eruptions on Alba Patera, Mars; Bulletin of volcanology, 50(6), 361-379.

[61] Lopes, R. M., Kilburn, C. R. (1990), Emplacement of lava flow fields: Application of terrestrial studies to Alba Patera, Mars; Journal of Geophysical Research: Solid Earth, 95(B9), 14383-14397.

[62] Greeley, R., and Hyde, J. (1972), Lava tubes of the Cave basalt, Mount St. Helens, Washington, Geol. Soc. Am. Bull., 83, 2397-2418.

[63] Riemers, C., and Komar, P. (1979), Evidence for explosive volcanic density currents on certain Martian volcanoes; Icarus, 39, 88-110.

[64] Greeley, R., and Crown, D. (1990), Volcanic geology of Tyrrhena Patera, Mars, J. Geophys. Res., 95, 7133-7149.

[65] Rampey, M. L., Milam, K. A., McSween Jr, H. Y., Moersch, J. E., Christensen, P. R. (2007), Identity and emplacement of domical structures in the western Arcadia Planitia, Mars; Journal of Geophysical Research: Planets, 112(E6).

[66] Farrand, W. H., Rice, J. W., Chuang, F. C., Rogers, A. D. (2020), Spectral and geological analyses of domes in western Arcadia Planitia, Mars: Evidence for intrusive alkali-rich volcanism and ice-associated surface features; Icarus, 114111.

[67] Brož, P., Hauber, E., Platz, T., Balme, M. (2015), Evidence for Amazonian highly viscous lavas in the southern highlands on Mars; Earth and Planetary Science Letters, 415, 200-212.

[68] Christensen, P. R., McSween, H. Y., Bandfield, J. L., Ruff, S. W., Rogers, A. D., et al. (2005), Evidence for magmatic evolution and diversity on Mars from infrared observations; Nature, 436(7050), 504-509.

[69] Wray, J. J., Hansen, S. T., Dufek, J., Swayze, G. A., Murchie, S. L., et al. (2013), Prolonged magmatic activity on Mars inferred from the detection of felsic rocks; Nature Geoscience, 6(12), 1013-1017.

[70] Calder, E. S., Lavallée, Y., Kendrick, J. E., Bernstein, M. (2015). Lava dome eruptions. In: The encyclopedia of volcanoes (pp. 343-362). Academic Press.

[71] Greeley, R., and Spudis, P. D. (1978), Volcanism in the cratered terrain hemisphere of Mars; Geophysical Research Letters, 5(6), 453-455.

[72] Walker, G. (1972), Compound and simple lava flows and flood basalts; Bull. Volcanol., 35, 579-590.

[73] Carr, M., and Schaber, G. (1977), Martian permafrost features; J. GeophysR. es., 82, 4039-4054.

[74] Guest, J. E., Butterworth, P. S., Greeley, R. (1977), Geological observations in the Cydonia region of Mars from Viking; Journal of Geophysical Research, 82(28), 4111-4120.

[75] Scott, D. (1979), Geologic problems in the northern plains of Mars, 10th Proc. Lunar Planet. Sci. Conf., 3039-3054.

[76] Hodges, C., and Moore, H. (1979), The subglacial birth of Olympus Mons and its aureoles; J. Geophys. Res., 84, 8061-8074.

[77] Lopes, R. M., Guest, J. E., Wilson, C. J. (1980). Origin of the Olympus Mons aureole and perimeter scarp. The moon and the planets, 22(2), 221-234.

[78] Platz, T., and Michael, G. (2011), Eruption history of the Elysium volcanic province, Mars; Earth and Planetary Science Letters, 312(1-2), 140-151.

[79] Plescia, J. B. (1990), Recent flood lavas in the Elysium region of Mars; Icarus, 88(2), 465-490.

[80] King, J. S., and Riehle, J. R. (1974). A proposed origin of the Olympus Mons escarpment. Icarus, 23(2), 300-317.

[81] Squyres, S. W., Wilhelms, D. E. Moosman, A. C. (1987). Large-scale volcano-ground ice interactions on Mars. Icarus, 70(3), 385-408.

[82] Glaze, L. S., Baloga, S. M., Garry, W. B., Fagents, S. A., Parcheta, C. (2009), A hybrid model for leveed lava flows: Implications for eruption styles on Mars; Journal of Geophysical Research: Planets, 114(E7).

[83] Hulme, G. (1974), The interpretation of lava flow morphology, Geophys. J. R. Astron. Soc., 39, 361– 383.

[84] Carr, M. H. (1974), The role of lava erosion in the formation of lunar rilles and Martian channels, Icarus, 22, 1 – 23

[85] Linneman, S. R., and A. Borgia (1993), The blocky andesitic lava flows of Arenal volcano, Costa Rica; In: Active Lavas, edited by R. J. Kilburn and G. Luongo, pp. 25–72, Routledge, London.

[86] Lipman, P. W., and N. G. Banks (1987), AA flow dynamics, Mauna Loa 1984, in Volcanism in Hawaii, edited by R.W. Decker et al., U.S. Geol. Surv. Prof. Pap., vol. 1350, pp. 1527–1567.

[87] Moore, H. J. (1987), Preliminary estimates of the rheological properties of 1984 Mauna Loa lava, in Volcanism in Hawaii, edited by R.W. Decker et al., in U.S. Geol. Surv. Prof. Pap., 1350, 1569– 1588

[88] Guest, J. E., Spudis, P., Greeley, R., Taylor, G., Baloga, S. (1995), Emplacement of xenolith nodules in the Kaupulehu lava flow, Hualalai Volcano, Hawaii; Bull. Volcanol., 57, 179– 184

[89] Garry, W. B. (2006), The emplacement of channeled flows in subaerial, submarine, simulated, and extraterrestrial environments, Ph.D. dissertation, 240 pp., State Univ. of New York at Buffalo, Buffalo.

[90] Carrigan, C. (2000) Plumbing systems; In: Encyclopedia of Volcanoes, Sigurdsson, H., et al. (eds.), Academic Press, p. 219-237.

[91] Wilson, L., and Head III, J. W. (2004), Evidence for a massive phreatomagmatic eruption in the initial stages of formation of the Mangala Valles outflow channel, Mars; Geophysical research letters, 31(15).

[92] Bonafede, M., and Mazzanti, M. (1997), Hot fluid migration in compressible saturated porous media; Geophysical Journal International, 128(2), 383-398.

[93] Head, J. W., Wilson, L., Mitchell, K. L. (2003), Generation of recent massive water floods at Cerberus Fossae, Mars by dike emplacement, cryospheric cracking, and confined aquifer groundwater release; Geophysical research letters, 30(11).

[94] Wilson, L., and Parfitt, E. A. (1990), Widths of dikes on Earth and Mars. In Mars: Evolution of Volcanism, Tectonics, and Volatiles (p. 308).

[95] Wilson, L., and Head, J. W. (1988), The influence of gravity on planetary volcanic eruption rates. In Lunar and Planetary Science Conference (Vol. 19).

[96] Rubin, A. (1993), Dikes vs. diapirs in viscoelastic rock; Earth Planet. Sci. Lett., 119.4, 641-659.

[97] Mouginis-Mark, P. J., and Wilson, L. (2019), Late-stage intrusive activity at Olympus Mons, Mars: Summit inflation and giant dike formation; Icarus, 319, 459-469.

[98] Scott, E. D., Wilson, L., Head, J. (2002), Emplacement of giant radial dikes in the northern Tharsis region of Mars. Journal of Geophysical Research: Planets, 107(E4), 3-1.

[99] Neukum, G., Jaumann, R., Hoffmann, H., Hauber, E., Head, J., et al. (2004), Recent and episodic volcanic and glacial activity on Mars revealed by the High Resolution Stereo Camera. Nature, 432(7020), 971-979.

[100] Robbins, S. J., Di Achille, G., Hynek, B. M. (2011). The volcanic history of Mars: High-resolution crater-based studies of the calderas of 20 volcanoes. Icarus, 211(2), 1179-1203.

[101] Parfitt, E. A., and J W. Head (1993), Buffered and unbuffered dike emplacement events on the Earth and Venus: Implications for the magma reservoir size, depth, and rate of magma replenishment; Earth, Moon, and Planets, 61(3), 249-281.

[102] Scott, E. D., and Wilson, L. (1999). Evidence for a sill emplacement event on the upper flanks of the Ascraeus Mons shield volcano, Mars. Journal of Geophysical Research: Planets, 104(E11), 27079-27089.

[103] Levy, J. S., Head, J. W., Marchant, D. R. (2009). Concentric crater fill in Utopia Planitia: History and interaction between glacial “brain terrain” and periglacial mantle processes. Icarus, 202(2), 462-476.

[104] Bramson, A. M., Byrne, S., Putzig, N. E., Sutton, S., Plaut, J. J., et al. (2015), Widespread excess ice in Arcadia Planitia, Mars. Geophysical Research Letters, 42(16), 6566-6574.

[105] Piqueux, S., Buz, J., Edwards, C. S., Bandfield, J. L., Kleinböhl, A., et al. (2019), Widespread Shallow Water Ice on Mars at High Latitudesand Midlatitudes. Geophysical Research Letters, 46(24), 14290-14298.

[106] Farrand, W. H., Lane, M. D., Edwards, B. R. (2008). North and south: Possible tuyas and hyaloclastite hills on the northern plains and in the southern dorsa argentea region of Mars. LPI, (1391), 1761.

[107] Ackiss, S., Horgan, B., Seelos, F., Farrand, W., Wray, J. (2018). Mineralogic evidence for subglacial volcanism in the Sisyphi Montes region of Mars. Icarus, 311, 357-370.

[108] Farrand, W. H., Lane, M. D., Edwards, B. R., Yingst, R. A. (2011), Spectral evidence of volcanic cryptodomes on the northern plains of Mars; Icarus, 211(1), 139-156.

[109] Squyres, S. W. (1979). The distribution of lobate debris aprons and similar flows on Mars. Journal of Geophysical Research: Solid Earth, 84(B14), 8087-8096.

[110] Mangold, N. (2003). Geomorphic analysis of lobate debris aprons on Mars at Mars Orbiter Camera scale: Evidence for ice sublimation initiated by fractures. Journal of Geophysical Research: Planets, 108(E4).

[111] Head, J. W., Nahm, A. L., Marchant, D. R., Neukum, G. (2006). Modification of the dichotomy boundary on Mars by Amazonian mid-latitude regional glaciation. Geophysical Research Letters, 33(8).

[112] Holt, J. W., Safaeinili, A., Plaut, J. J., Young, D. A., Head, J. W., et al. (2008). Radar sounding evidence for ice within lobate debris aprons near Hellas Basin, mid-southern latitudes of Mars. LPI, (1391), 2441.

[113] Bills, B. G., and Ferrari, A. J. (1978). Mars topography harmonics and geophysical implications. Journal of Geophysical Research: Solid Earth, 83(B7), 3497-3508.

[114] Stevenson, D. J., Spohn, T., Schubert, G. (1983). Magnetism and thermal evolution of the terrestrial planets. Icarus, 54(3), 466-489.

[115] Comer, R., Solomon, S. C., Head, J. W. (1985). Mars: Thickness of the lithosphere from the tectonic response to volcanic loads. Reviews of Geophysics, 23(1), 61-92.

[116] Elder, J. W. (1987), The Structure of the Planets; Academic, San Diego, Calif., 210 pp.

[117] Solomon, S. C., and J. W. Head (1990), Heterogeneities in the thickness of the elastic lithosphere of Mars: Constraints on heat flow and internal dynamics, J. Geophys. Res., 95, 11,073-11,083.

[118] Oxburgh, E. R. (1980), Heat flow and magma genesis, in Physics of Magmatic Processes, edited by R. B. Hargraves, pp. 161-199, Princeton University Press, Princeton, N.J.

[119] Sleep, N. (1988), Tapping of melt by veins and dikes, J. Geophys. Res., 93, 10,255-10,272.

[120] Marsh, B., Carmichael, I. (1974), Benioff zone magmatism, J. Geophys. Res., 79, 1196-1206, 1974.

[121] Marsh, B. D., and Kantha, L. (1978), On the heat and mass transfer from an ascending magma, Earth Planet. Sci. Lett., 39, 435-443.

[122] Spera, F. J. (1980), Aspects of magma transport, in Physics of Magmatic Processes, edited by R. B. Hargraves, pp.265-323, Princeton University Press, Princeton, N.J.

[123] Wilson, L., Scott, E. D., Head, J. W. (2001). Evidence for episodicity in the magma supply to the large Tharsis volcanoes. Journal of Geophysical Research: Planets, 106(E1), 1423-1433.

[124] Marsh, B. (1984). Mechanics and energetics of magma formation and ascension. Studies in Geophysics. Explosive Volcanism: Inception, Evolution, and Hazards, 67-83.

[125] Blake, S. (1981), Volcanism and the dynamics of open magma chambers, Nature, 289, 783-785.

[126] Walker, G. P. L., S. Self, and L. Wilson (1984), Tarawera, 1886, New Zealand---A basaltic plinian fissure eruption, J. Volcanol. Geotherm. Res., 21, 61-78.

[127] Gudmundsson, A. (1990). Emplacement of dikes, sills and crustal magma chambers at divergent plate boundaries. Tectonophysics, 176(3-4), 257-275.

[128] Ryan, M.P. (1987), Neutral buoyancy and the mechanical evolution of magmatic systems, in Magmatic Processes: Physiochemical Principles, edited by B. O. Mysen, Spec. Publ. Geochem. Soc., 1,259-287.

[129] Rubin, A. M., and Pollard, D. D. (1987). Origins of blade-like dikes in volcanic rift zones. US Geological Survey Professional Paper, 1350(2), 1449-1470.

[130] Lipman, P. (2000) Calderas; In: Encyclopedia of Volcanoes, Sigurdsson, H., et al. (eds.), Academic Press, p. 643-663.

[131] Zimbelman, J. R., and Edgett, K. S. (1992). The Tharsis Montes, Mars: Comparison of volcanic and modified landforms. In Proceedings of Lunar and Planetary Science, volume 22. Lunar and Planetary Institute.

[132] Crumpler, L. S., Head, J. W., Aubele, J. C. (1994). Calderas on Mars: Classification, characteristics, and processes related to mechanisms of formation. In Lunar and Planetary Science Conference (Vol. 25, p. 305).

[133] Crumpler, L. S., Head, J. W., Aubele, J. C. (1996). Calderas on Mars: Characteristics, structure, and associated flank deformation. Geological Society, London, Special Publications, 110(1), 307-348.

[134] Zimbelman, J. (2000) Volcanism on Mars; In: Encyclopedia of Volcanoes, Sigurdsson, H., et al. (eds.), Academic Press, p. 771 – 783.

[135] Marti, J., Ablay, G. J., REDSHAW, L. T., Sparks, R. S. (1994). Experimental studies of collapse calderas. Journal of the Geological society, 151(6), 919-929.

[136] Mouginis-Mark, P. J., and Robinson, M. S. (1992). Evolution of the Olympus Mons Caldera, Mars. Bulletin of Volcanology, 54(5), 347-360.

[137] Zuber, M. T., and Mouginis-Mark, P. J. (1992). Caldera subsidence and magma chamber depth of the Olympus Mons volcano, Mars. Journal of Geophysical Research: Planets, 97(E11), 18295-18307.

[138] Mouginis-Mark, P. J. (1990). Recent water release in the Tharsis region of Mars. Icarus, 84(2), 362-373.

[139] Holcomb, R. T. (1987), Eruptive history and long-term behavior of Kilauea Volcano, in Volcanism in Hawaii, edited by R. W. Decker et al., U.S. Geol. Surv. Prof. Pap., 1350, 261– 350.

[140] Scott, D., and Carr, M. (1978), Geologic map of Mars, scale 1:25,000,000, U.S. Geol. Surv. Misc. Invest. Ser., Map I-1083.

[141] Carr, M. H. (1976). The volcanoes of Mars. Scientific American, 234(1), 32-43.

[142] Wood, C. A. (1984). Calderas: a planetary perspective. Journal of Geophysical Research: Solid Earth, 89(B10), 8391-8406.

[143] Plescia, J. B. (2004), Morphometric properties of Martian volcanoes, J. Geophys. Res., 109, E03003

[144] Kerber, L., Head, J. W., Madeleine, J. B., Forget, F., Wilson, L. (2011). The dispersal of pyroclasts from Apollinaris Patera, Mars: Implications for the origin of the Medusae Fossae Formation. Icarus, 216(1), 212-220.

[145] Lipman, P. (1997). Subsidence of ash-flow calderas: relation to caldera size and magma-chamber geometry. Bulletin of volcanology, 59(3), 198-218.

[146] Mason, B. G., Pyle, D. M., Oppenheimer, C. (2004). The size and frequency of the largest explosive eruptions on Earth. Bulletin of Volcanology, 66(8), 735-748.

[147] Scott, D. H., Dohm, J. M., Applebee, D. J. (1993). Geologic map of science study area 8, Apollinaris Patera region of Mars. USGS, 2351.

[148] Robinson, M. S., Mouginis-Mark, P. J., Zimbelman, J. R., Wu, S. S., Ablin, K. K., Howingtonkraus, A. E. (1993). Chronology, Eruption Duration, and Atmospheric Contribution of the Martian Volcano Apollinaris-Patera. Icarus, 104, 301-323.

[149] Farrell, A. K., and Lang, N. P. (2010). Distribution of explosive and effusive volcanic deposits at Apollinaris Patera, Mars. LPI, (1533), 2072.

[150] Crown, D. A., and Greeley, R. (1989). The martian highland Paterae: evidence for explosive volcanism on Mars. In MEVTV Workshop on Early Tectonic and Volcanic Evolution of Mars (pp. 29-31).

[151] Hauber, E., van Gasselt, S., Ivanov, B., Werner, S., Head, J. W., et al. (2005). Discovery of a flank caldera and very young glacial activity at Hecates Tholus, Mars. Nature, 434(7031), 356-361.

[152] Neukum, G., and Hiller, K. (1981). Martian ages. Journal of Geophysical Research: Solid Earth, 86(B4), 3097-3121.

[153] Malin, M. C., and Dzurisin, D. (1977). Landform degradation on Mercury, the Moon, and Mars: Evidence from crater depth/diameter relationships. Journal of Geophysical Research, 82(2), 376-388.

[154] Walker, G. (1973), Lengths of lava flows; Philos. Trans. R. Soc. London, Ser. A, 274, pp. 107-118

[155] Hulme, G. (1976). The determination of the rheological properties and effusion rate of an Olympus Mons lava. Icarus, 27(2), 207-213.

[156] McGetchin, T. R., and Smith, J. R. (1978). The mantle of Mars: Some possible geological implications of its high density. Icarus, 34(3), 512-536.

[157] Cataldo, V., Williams, D.A., Schmeeckle, M.W., and Leone, G. (2019). Vallis Schröteri, Moon: Results of first 3-D model of thermal erosion by turbulently flowing lava reveal how erosion likely shaped the inner rille. 50th Lunar and Planetary Science Conference, abstract #2297.

[158] Moukalled, F., Mangani, L., Darwish, M., (2015), The finite volume method in computational fluid dynamics: An advanced introduction with OpenFOAM and Matlab. Ed. 1, Springer Internat. Publish.

[159] Jones, W.P., Launder, B.E., (1972), The prediction of laminarization with a two-equation model of turbulence. Intern. J. of Heat and Mass Transfer, 15, pp. 301-314. Kakaç, S., Shah, R.K., Aung, W., 1987. Handbook of Single-Phase Convective Heat Transfer, John Wiley & Sons, New York.

[160] Launder, B.E., Sharma, B.I., (1974), Application of the energy dissipation model of turbulence to the calculation of flow near a spinning disk. Letters of Heat and Mass Transfer, 1, n. 2, pp. 131-138.

[161] Menter, F.R., (1993), Zonal two-equation k-ω turbulence models for aerodynamic flow. AIAA paper, 93-2906.

[162] Patankar, S. V. and Spalding, D.B., (1972). A calculation procedure for heat, mass and momentum transfer in three-dimensional parabolic flows. Int. J. of Heat and Mass Transfer, Vol. 15, 10, pp. 1787-1806.

[163] Hulme, G. (1973), Turbulent lava flow and the formation of lunar sinuous rilles Mod. Geol., 4, pp. 107-117.

[164] Huppert, H.E., Sparks, R.S.J., (1985). Komatiites, I, Eruption and flow. J. Petrol. 26, pp. 694–725.

[165] Williams, D. A., Kerr, R. C., Lesher, C. M. (1998). Emplacement and erosion by Archean komatiite lava flows at Kambalda: revisited. Journal of Geophysical Research: Solid Earth, 103(B11), 27533-27549.

[166] Williams, D.A., Fagents, S.A., Greeley, R.A., (2000), A reassessment of the emplacement and erosional potential of turbulent, low-viscosity lavas on the Moon. J. Geophys. Res. 10520(E8), pp. 189–205

[167] Kakac, S., Yener, Y., Pramuanjaroenkij, A. (2013). Convective heat transfer. CRC press.

[168] Dragoni, M., Bonafede, M., Boschi, E., (1986), Downslope flow models of a Bingham liquid: Implications for a lava flow. J. Volcanol. Geotherm. Res., v. 30, p. 305-325. Hulme, G., 1973. Turbulent lava flows and the formation of lunar sinuous rilles. Mod. Geol. 4, pp. 107-117.

[169] Kerr, R.C., (2001). Thermal erosion by laminar lava flows. J. Geophys. Res. 106, B11, 26.453-26,465.

[170] Siewert, J., Ferlito, C., (2008). Mechanical erosion by flowing lava. Contemp. Phys. 49, pp. 43 –54, doi:10.1080/00107510802077388.

[171] Wilson, L., Head, J.W., (2017). Generation, ascent and eruption of magma on the Moon: New insights into source depths, magma supply, intrusions and effusive/explosive eruptions (Part 1: Theory). Icarus, 283, 146-175.

[172] Masson, P. (1977), Structure pattern-analysis of Noctis Labyrinthus-Valles Marineris regions of Mars. Icarus, 30 (1), 49-62.

[173] Schultz, R. (1991), Structural development of Coprates Chasma and western Ophir Planum, Valles Marineris rift, Mars. J. Geophys. Res. Planet., 96 (E5), 22777-22792.

[174] Wilkins, S., and Shultz, R. (2003), Cross faults in extensional settings: Stress triggering, displacement localization, and implications for the origin of blunt troughs at Valles Marineris, Mars. J. Geophys. Res. Planets, 108 (E6).

[175] Leone, G. (2014), A network of lava tubes as the origin of Labyrinthus Noctis and Valles Marineris on Mars. J. Volcanology and Geothermal Res., 277, 1-8.

[176] Cushing, G., Titus, T., Wynne, J., Christensen, P. (2007), THEMIS observes possible cave skylights on Mars. Geophys. Res. Lett., 34 (17).

[177] Leveille, R. and Datta, S., (2010), Lava tubes and basaltic caves as astrobiological targets on Earth and Mars: a review. Planet. Space Sci., 58 (4), 592-598.